URSI GASS 2021, Rome, Italy, 28 August - 4 September 2021

Increase of exposure levels due to antenna/body coupling in the 60-GHz band

M. Ziane[(1)], M. Zhadobov* [(1)], and R. Sauleau[(1)]
(1) Univ Rennes, CNRS, IETR (Institut d'Électronique et des Technologies du numéRique), UMR 6164, F-35000, Rennes, France.

Abstract

When an antenna is located close to a lossy medium, near-field interactions appear and may modify the incident electromagnetic field. In this stydy, we analyse for the first time analyticaly and numericaly the impact of antenna/human body interactions on the absorbed power density (APD) at 60 GHz using a skin-equivalent model. To this end, equivalent sources and patch antenna arrays are used. The results demonstrate that the antenna/body interactions result in an increase of the average APD (increase up to 84.1%, 98.3%, and 103.3% for adult dry, adult wet, and children skin, respectively) and modification of its spatial distribution. These results suggest that APD is underestimated in free-space measurements and that accurate experimental dosimetry requires taking into account the presence of the human body.

1 Introduction

The evolution of communication devices and saturation of the microwave spectrum leads to the increasing exploitation of the millimeter-wave (mmW) spectrum. In particular, the 60-GHz band has been identified as an attractive solution for radio access and backhauling in future mmW systems. Wireless devices, such as smartphones or tablets, which are intended to be used in the vicinity of the human body, have to comply with the exposure limits. In the 6–300 GHz range, the absorbed power density and epithelial power density are used as the main dosimetric quantities [1, 2]. Both the ICNIRP and IEEE set the limits to 10 mW/cm^2 for occupational environments (referred as restricted environments in the IEEE standard), and 2 mW/cm^2 for the general public (referred as unrestricted environments in the IEEE standard). Above 6 GHz, the power density is to be averaged over 4 cm^2 and 6 min. Moreover, from 30 to 300 GHz, the power density averaged over 1 cm^2 must not exceed two times the exposure limit for 4 cm^2.

The existing dosimetry systems [3]–[5] are designed to measure the incident power density in free-space close to a wireless device under test. However, when an antenna is located in the vicinity of a lossy medium, electromagnetic contrast at the air/lossy medium interface results in appearance of a scattered field and near field interactions, modifying the field impinging the human body [6]. Hence, in free-space measurements of the incident power density variations of the power density due to the coupling of a wireless device with the human body are not taken into account.

The main purpose of this study is to analyze the impact of the antenna/human body interactions in the near-field on the absorbed power density (APD) at 60 GHz. Equivalent sources and patch antenna arrays are compared. The role of the reflection coefficient from skin, antenna directivity and ground plane dimensions are also investigated.

2 Exposure scenarios

To analyze variations of APD in a homogeneous skin-equivalent model due to the presence of a radiating structure, the considered exposure scenarios are depicted I, Figure 1.

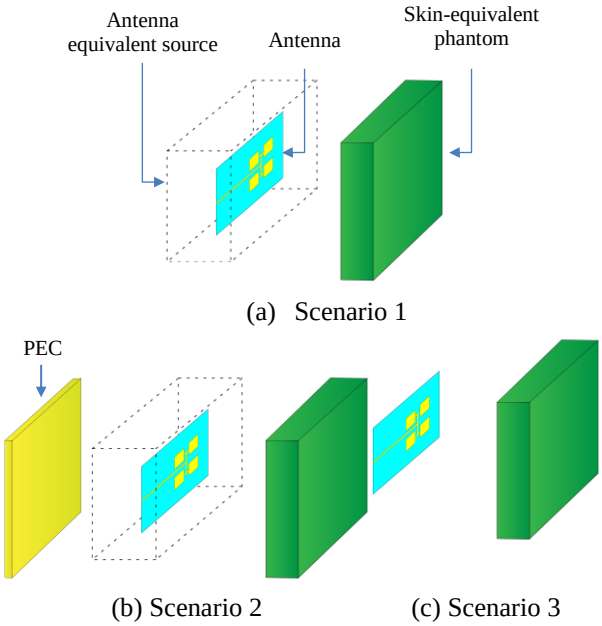

Figure 1. Exposure scenarios.

Scenario 1: An antenna equivalent source representing a single or four-patch antennas arrays radiating towards a semi-infinite flat skin-equivalent model (Figure 1a). In this scenario, the impact of the scattered from the phantom field on the antenna performances is neglected.

Because of the shallow penetration depth at mmWs (<1 mm), a homogenous skin-equivalent layer is used as a model [7]. The dielectric properties of the skin model are those of dry skin at 60 GHz extracted from [8]. For

completeness, we also provide the main results for wet skin (Table 1) [8].

Table 1. Skin model complex permittivity and reflection coefficient

Skin model	*Permittivity (ε)*	*Amplitude reflection coefficient (|R|)*
Adult (dry)	07.98 − j10.90	0.6145
Adult (wet)	10.22 − j11.83	0.6296

Scenario 2: Scenario 1 with a perfect electric conductor (PEC) parallel to the skin model (Figure 1b) to simulate the case where the free-space antenna matching, efficiency, and radiated field are preserved and not modified by the phantom.

Scenario 3: Patch antennas placed in the vicinity of the skin model (Figure 1c). The source main beam is directed towards the phantom representing the worst-case exposure scenario. The following sources have been considered: single patch antenna (SPA) and patch antenna array with 4 radiating elements (2×2 PAA), inspired from [9] (Figure 2) and matched to 50 Ω in free-space at 60 GHz. All results are provided for an antenna input power of 10 mW.

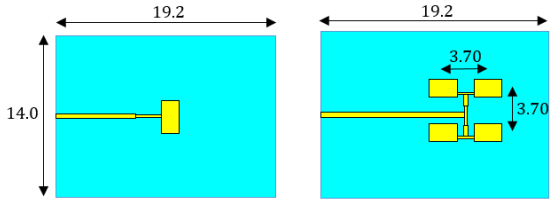

(a) (b)

Figure 2. Antenna topologies: (a) single patch antenna (SPA); (b) 2×2 patch antenna array (2×2 PAA). Dimensions are in mm.

3 Methods

The analytical and numerical methods used for exposure assessment.

3.1 Analytical method

In scenarios 1 and 2, APD is calculated using the plane-wave spectrum theory (PWS) [11, 12]. It represents the spatial distribution of each field component over a transverse plane as a superposition of the plane waves propagating along different directions defined by the couplet $\boldsymbol{K} = k_x\hat{x} + k_y\hat{y}$. The PWS of an electric field phasor component $\boldsymbol{E}(\boldsymbol{R}, z_0)$ over a plane Ψ identified by $z = z_0$ and $\boldsymbol{R} = x\hat{x} + y\hat{y}$ is expressed as

$$\widehat{\boldsymbol{E}}(\boldsymbol{K}, z_0) = \int_{\boldsymbol{R}} \boldsymbol{E}(\boldsymbol{R}, z_0) e^{j\boldsymbol{K}\cdot\boldsymbol{R}} d\boldsymbol{R}\,. \qquad (1)$$

The tangential spectrum components of the incident ($\widehat{\boldsymbol{E}}^{||}_{\boldsymbol{inc}}$) and transmitted fields ($\widehat{\boldsymbol{E}}^{||}_{tr}$) at the air/phantom interface are related as follows

Scenario 1:

$$\widehat{\boldsymbol{E}}^{||}_{tr}(\boldsymbol{K}) = \boldsymbol{\Pi_1}\widehat{\boldsymbol{E}}^{||}_{\boldsymbol{inc}}(\boldsymbol{K}). \qquad (2)$$

Scenario 2:

$$\widehat{\boldsymbol{E}}^{||}_{tr}(\boldsymbol{K}) = \boldsymbol{\Pi_1}(I + e^{-2jk_z d}\boldsymbol{\Gamma_1})^{-1}\widehat{\boldsymbol{E}}^{||}_{\boldsymbol{inc}}(\boldsymbol{K}) \qquad (3)$$

where $\boldsymbol{\Pi_1}$ and $\boldsymbol{\Gamma_1}$ are the spectral transmission and reflection coefficients at the air/phantom interface given in [10], I is the identity matrix, k_z is the longitudinal propagation constant given as $k_z = \sqrt{k^2 - |\boldsymbol{K}|^2}$ with k is the propagation constant, and d is the PEC–phantom separation distance.

The normal field spectrum component is obtained from the tangential field spectra $\widehat{\boldsymbol{E}}^{||}$ using the Gauss law

$$\widehat{\boldsymbol{E}}_{\boldsymbol{z}} = -\frac{\boldsymbol{K}\cdot\widehat{\boldsymbol{E}}^{||}}{k_z} \qquad (4)$$

The H-field spectrum is calculated as [12]

$$\widehat{\boldsymbol{H}}_{tr} = \frac{1}{\mu\omega}(\boldsymbol{k}) \times (\widehat{\boldsymbol{E}}_{tr}) \qquad (5)$$

The spatial field components ($\boldsymbol{E}$ and $\boldsymbol{H}$) are retrieved using the inverse Fourier transform of the field spectra. The APD is calculated as [1]

$$APD = \iint_A Re[\boldsymbol{E} \times \boldsymbol{H}^*] \cdot \frac{\boldsymbol{ds}}{A} \qquad (6)$$

where ds is the integral variable vector with the normal direction to the integral area A on the body surface. All results are provided for an averaging area A of 1 cm^2 (except 2-dimensional APD distributions provided in sections 4.2). Note that the APD is identical to the epithelial power density as defined by [2].

3.2 Numerical method

Scenario 3 was analyzed numerically using the finite integration technique (FIT) implemented in CST Microwave Studio.

4 Results

To analyze the APD variations due to the antenna/body coupling, the following figures of merit are defined

$$\Upsilon_{(2,1)} = \frac{APD_2}{APD_1} \qquad (7)$$

$$\Upsilon_{(3,1)} = \frac{APD_3}{APD_1} \qquad (8)$$

where $\boldsymbol{APD_1}$, $\boldsymbol{APD_2}$, and $\boldsymbol{APD_3}$ are APD from scenarios 1, 2, and 3, respectively.

4.1 Equivalent sources

Here, we consider the equivalent sources corresponding to the single patch and four-patch antenna array (scenarios 1 and 2). $\Upsilon_{(2,1)}$ is calculated from Equations (1)–(7) for the dry skin model using 2×2 PAA (Figure 3a).

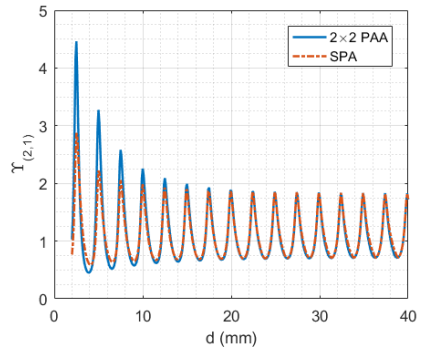

(**a**)

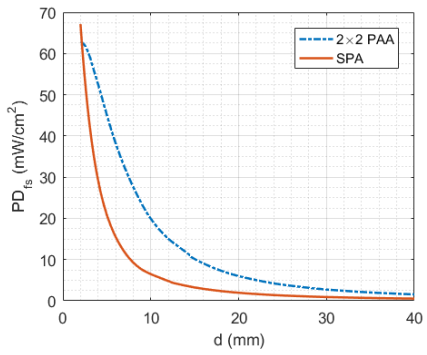

(**b**)

Figure 3. Equivalent sources: (a) $\Upsilon_{(2,1)}$; (b) Free-space peak power density.

Significant differences in $\Upsilon_{(2,1)}$ maxima and, to a smaller extent, minima between the antenna-equivalent sources are noted for d < 20 mm (Figure 3a). The APD increases (decreases) up to (down to) 174% (39%), 342% (54%), for the SPA, and 2×2 PAA, respectively. This is due to the differences in the attenuation rate of the peak power density in free-space PD_{fs} of the antenna-equivalent sources (Figure 3b). Indeed, when the PD_{fs} attenuation rate is higher, $\Upsilon_{(2,1)}$ is lower. $\Upsilon_{(2,1)}$ of both antenna-equivalent sources converges with d to $1/d^2$oscillatory function (free-space power density decrease in the far-field).

The APD increase is proportional to the reflection coefficient at the air/skin interface (APD increase up to 373.4% for the wet skin model).

4.2 Patch antennas

When an antenna is located in the vicinity of a scatter, its matching and radiation characteristics are altered. To exclude the effect of the antenna mismatch, APD_3 is normalized to $(1\text{-}S_{11/Ph}{}^2)$ and APD_1 to $(1\text{-}S_{11/FS}{}^2)$, where $S_{11/Ph}$ and $S_{11/FS}$ are S_{11} of the antenna in the presence of the phantom and in free space, respectively. Note that modern wireless devices are equipped with matching networks designed to compensate for the mismatch.

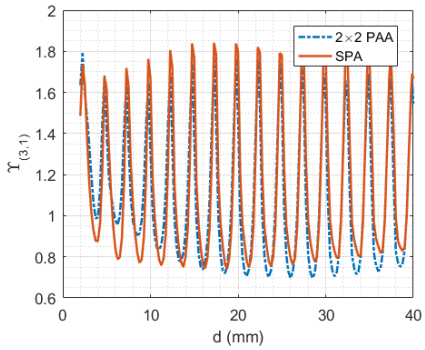

Figure 4. $\Upsilon_{(3,1)}$ for the patch antennas.

The changes in the APD due to the antenna/phantom coupling (scenarios 1 and 3) are shown in Figure 4. The APD increases up to (decrease down to) 84.11% (25.7 %) and 79.2 (30.1%) for SPA and 2×2 PAA, respectively. The variations are higher for wet skin (increase up to 98.25% and decrease down to 32.5%) and children (increase up to 103.3% and decrease down to 33.7%).

The results shown in Figure 4 demonstrate that there is no direct correlation between $\Upsilon_{(3,1)}$ and the source directivity even for short d as seen in scenario 2 (Figure 3a). Indeed, $\Upsilon_{(3,1)}$ is lower compared to $\Upsilon_{(2,1)}$. This difference is attributed, to a smaller extent, to losses inside the antenna (18.6%, with respect to the total accepted power at $d = 2.25$ mm) and, to a larger extent, to the scattering properties of the antennas. The higher the scattering, the lower the APD variations.

Note that the ground plane size impacts the APD variations. For instance for the SPA, the APD variations increase with size until the ground plane becomes large enough (e.g., for ground plane dimensions of 2.5×2.5 to 10×10 mm^2, $\Upsilon_{(7,5)}$ increases from 10% to 79%).

Furthermore, we analyzed the impact of the near-field interactions on the spatial APD distribution for the 2×2 PAA (Figure 6). The distribution of APD_3 is affected by the antenna/phantom interactions and evolves with d. For d corresponding to the maximum APD (i.e., 9.75 mm), the absorbed power density is concentrated around its maximum. It extends progressively over a larger surface when d approaches the value corresponding to APD minima (i.e., 8.75 mm). When the spatial distribution of APD is concentrated around its maxima, the spatial averaging area has a stronger impact on the mean APD, which rapidly decreases with the averaging area (e.g., the ratio between APD averaged over 1 cm^2 and 4 cm^2 equals to 2.86 and 3.17 for d = 8.75 and 9.75 mm, respectively).

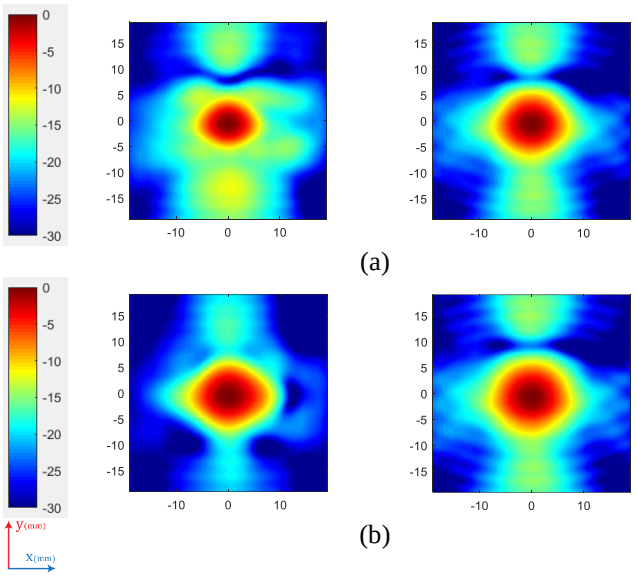

Figure 6. APD distribution for 2×2 PAA (scenario 3, left column) and 2×2 PAA equivalent source without PEC (scenario 1, right column): (a) d=8.75 mm; (b) d=9.75 mm.

5 Conclusion

We analyzed the impact of the near-field antenna/body interactions on APD at 60 GHz. The results show that the presence of the body in the vicinity of a source results in a modification, mainly increase, of the average APD. For the antenna-equivalent sources, the presence of a PEC increases the APD up to (decreases down to) 342% (54%), for the 2×2 PAA. For realistic antenna, APD increases up to 84.11% and decreases down to 30.1% for SPA and 2×2 PAA, respectively. The variations are higher for wet skin (increase up to 98.25%) and children (increase up to 103.3%). In addition to the peak APD, it was shown that the spatial distribution of APD is impacted by the presence of the tissue-equivalent phantom and depends on the separation distance. These results suggest that the exact peak value and distribution of APD cannot be retrieved from measurements of the incident power density in free-space in absence of the body model.

6 Acknowledgements

This work was supported by the French National Research Program for Environmental and Occupational Health of ANSES (2018/2 RF/07) through NEAR 5G project.

7 References

[1] International Commission on Non-Ionizing Radiation Protection (ICNIRP)1, « Guidelines for Limiting Exposure to Electromagnetic Fields (100 kHz to 300 GHz) »:, *Health Phys.*, vol. 118, nº 5, p. 483-524, mai 2020.

[2] « IEEE Standard for Safety Levels with Respect to Human Exposure to Electric, Magnetic, and Electromagnetic Fields, 0 Hz to 300 GHz », IEEE.

[3] S. Pfeifer *et al.*, « Total Field Reconstruction in the Near Field Using Pseudo-Vector E-Field Measurements », *IEEE Trans. Electromagn. Compat.*, vol. 61, nº 2, p. 476-486, avr. 2019.

[4] P. Noren, L. J. Foged, L. Scialacqua, et A. Scannavini, « Measurement and Diagnostics of Millimeter Waves 5G Enabled Devices », in *2018 IEEE Conference on Antenna Measurements & Applications (CAMA)*, Västerås, sept. 2018, p. 1-4.

[5] M. Nesterova et S. Nicol, « Analytical Study of 5G Beamforming in the Reactive Near-Field Zone », in *12th European Conference on Antennas and Propagation (EuCAP 2018)*, London, UK, 2018, p. 727 (5 pp.)-727 (5 pp.).

[6] B. Derat et A. Cozza, « Analysis of the transmitted field amplitude and SAR modification due to mobile terminal flat phantom multiple interactions », in *2nd European Conference on Antennas and Propagation (EuCAP 2007)*, Edinburgh, UK, 2007, p. 186-186.

[7] A. R. Guraliuc, M. Zhadobov, R. Sauleau, L. Marnat, et L. Dussopt, « Millimeter-wave electromagnetic field exposure from mobile terminals », in *2015 European Conference on Networks and Communications (EuCNC)*, Paris, France, juin 2015, p. 82-85.

[8] S. Gabriel, R. W. Lau, et C. Gabriel, « The dielectric properties of biological tissues: II. Measurements in the frequency range 10 Hz to 20 GHz », *Phys. Med. Biol.*, vol. 41, nº 11, p. 2251–2269, nov. 1996.

[9] C. Leduc et M. Zhadobov, « Impact of Antenna Topology and Feeding Technique on Coupling With Human Body: Application to 60-GHz Antenna Arrays », *IEEE Trans. Antennas Propag.*, vol. 65, nº 12, p. 6779-6787, déc. 2017.

[10] A. Cozza et B. Derat, « On the Dispersive Nature of the Power Dissipated Into a Lossy Half-Space Close to a Radiating Source », *IEEE Trans. Antennas Propag.*, vol. 57, nº 9, p. 2572-2582, sept. 2009.

[11] C. Scott, *The spectral domain method in electromagnetics*. Norwood, MA: Artech House, 1989.

[12] S. Gregson, J. McCormick, et C. Parini, *Principles of Planar Near-Field Antenna Measurements*. The Institution of Engineering and Technology, Michael Faraday House, Six Hills Way, Stevenage SG1 2AY, UK: IET, 2007.